Approximate Power Flow Solutions-Based Forecasting-Aided State Estimation for Power Distribution Networks

Zhenyu Wang[1], Zhao Xu[2], Donglian Qi[1,3*], Yunfeng Yan[1], and Jianliang Zhang[1]
[1]College of Electrical Engineering, Zhejiang University, Hangzhou, China
[2]Department of Electrical Engineering, The Hong Kong Polytechnic University, Hong Kong, China
[3]Hainan Institute of Zhejiang University, Sanya, China
*Corresponding author e-mail: qidl@zju.edu.cn

***Abstract*—Emerging forecasting-aided state estimation (FASE) frequently encounters complicated parameter analysis and observation calculation tasks, especially when confronted with intricate and uncertain scenarios. To this end, a concise FASE estimator is developed by combining the precise depiction of dynamic state change and linear power flow approximation. Designing the dynamic system state as a voltage perturbation vector around the nominal value, the forecasted state is firstly derived from the linear approximation of power injection equation solutions. The state forecasting model relies solely on nodal impedance information as the state transition matrix, eliminating the onerous parameter tuning effort. After that, the optimal filtered state is efficiently obtained utilizing line power flow measurements, with branch admittance information to construct the approximate observation matrix. Numerical simulation comparisons on a symmetric balanced 56-node distribution system verify the performance of the proposed estimator in terms of accuracy and robustness.**

***Index Terms*—Distribution networks, forecasting-aided state estimation, approximate power flow, linear approximation.**

I. Introduction

IN modern power distribution systems, the state estimation (SE) plays a crucial role in ensuring reliable operation and enhancing the intelligence level [1]–[3]. However, the power system undergoes a dynamic changing process with load variations followed by generation adjustments, posing significant challenges for normal operating conditions [4]. In particular, with the uncertain fluctuations in power scheduling and increased participation of distributed generations (DGs), the system state may experience sudden changes due to their stochastic and intermittent characteristics. For instance, power injection changes at the buses of load or DG can cause the voltage phase angle to fluctuate rapidly in a short timeframe [5]. Therefore, the forecasting-aided state estimation (FASE) methods [6] are necessarily developed to predict and track the dynamic system changing between multiple time scales.

For static SE tools, the current system state is estimated with redundant measurements from the power system SCADA at one specific time. Considering more dynamic drivers, i.e., load and generation power variations, FASE estimators describe the slow-time evolution of the static state within a period. Initially, the naive FASE models only using one-step ahead forecasting method were proposed [7], but the limited forecasting ability restricted their performance. Then, the innovation analysis was introduced to filtering stage to handle inaccurately forecasted states and identify outliers simultaneously [8]. This contributed to the classic FASE modeling paradigm encompassing state transition-based forecasting and measurement-based filtering.

In state forecasting process, the time series analysis models occupy an important position. A research summary on converting time series models to state space form can be found in [9]. Therein, Holt's two-parameter exponential smoothing [10] and auto-regressive (AR) models [11] are the most used to forecast short-term system states. For example, accompanying the AR prediction method, the optimal PMU placement is configured to provide the filtered states of voltage and current amplitude in [11]. Holt's two-parameter exponential smoothing method is employed to cooperate with the interactive multiple model (IMM) algorithms and finally output the joint results in [12]. In [13], the Holt's method combined with minimum error entropy filtering provides abnormal operating situation estimations considering sudden loads state changes and measurement failures. And the spatial and temporal correlations of load and DGs are considered in [4]. By estimating the probability density functions of Holt's method-based state space, the accuracy missed in linearization of nonlinear measurement equations is improved in [14]. From above, the primary motivation behind the improvements is to compensate for the shortcomings in prediction ability, albeit at the increased cost of execution complexity in the filtering process. Even when more robust prediction models account for additional uncertain factors [2], [13], [15], [16], their statistical models necessitate extensive parameter tuning to align with historical data under implicit assumptions, which thwarts an adaptive application.

In state filtering process, the filtered state along with power measurements are interrelated within the power flow equations. Given the power measurements of generators and loads, voltage values obtained from power flow solutions effectively describe the operational states [17]. However, directly obtaining analytic solutions to the power flow equation poses a challenging task due to the intractable nonlinear term [18]. Especially in a distribution power system where the feeders are not purely inductive, voltage magnitude and phase angle are entangled within the power flow equations. Thus, explicit approximate solutions of nonlinear power equations

are proposed with the practical linearization assumption. For example, linear approximations of power flow solutions in distribution networks with the fixed point theorem is studied in [18], namely the system state can be approximated based on power flow or injection measurements without too much effort. Then, the false data injection cyber-attacks based on that are analysed in [19]. The approximation of optimal power flow solution is investigated in [20]–[22], primarily reduced model complexity without sacrificing accuracy. However, the above are all bound in static SE without considering the dynamic forecasted-aid factors. On the other hand, the precise measurement scheme is also introduced to improve the state filtration efficiency. For example, the performance assessment of filtering correction through only PMU measurements is provided in [11], and the mixed measurements with RTU are studied in [23] to handle asynchronous characteristics and improve computational accuracy. But the realistic cost of high-precision meters hinders its widespread application. Therefore, to solve aforementioned problems, it is worth incorporating dynamic factors into the performance advantage of approximate power flow models to develop the lightweight FASE estimator.

In this paper, we propose an efficient and concise FASE estimator based on approximate linear power flow models (APF-FASE). The goal is to introduce dynamic power variations into the proposed approximate power flow model and integrate them into the FASE framework for explicitness and efficiency. The proposed estimator derives the approximate power flow solutions as the predicted and filtered states without much effort. This approach is sufficient for normal operating scenarios and aids in mitigating the adverse effects of sudden state changes and false measurements. The contributions of this paper are summarized below.

1) We design real and imaginary parts of a voltage perturbation vector around the nominal value as the system dynamic variable to replace the overall expression of nodal voltage. More detailed depictions of state changes are beneficial for improving estimator accuracy. In addition, its robustness against sudden state changes and false measurements is validated.
2) Different from most existing works, the proposed estimator employs an approximate power injection model in forecasting stage incorporating with the dynamic power variations. The concise forecasting model is only based on nodal impedance information, eliminating the complex parameter-matching processes in comparison with the traditional time series analysis models. Numerical results demonstrate that voltage states can be accurately forecasted with the dynamic linear approximation.
3) For state filtering, the approximate line power flow measurement equation is selected instead of traditional nonlinear power flow formulas. In close collaboration with the proposed prediction model, state filtering can be implemented using only line power flow measurements and branch admittance information. Numerical results demonstrate that the filtering performance is comparable to full-information nonlinear equations but without iterative complexity of nonlinear calculations.

The rest of this paper is organized as follows. Section II describes the mathematical models of single-phase feeder and FASE in power distribution systems. Section III introduces the static approximations to distribution system state based on power injection and flow measurements. Section IV presents the proposed dynamic FASE estimator with the approximate system state. The numerical simulation results based on IEEE test feeder with different operational scenarios are discussed in Section V, and the conclusion is rendered in Section VI.

II. Mathematical Modeling

In this paper, the following notations are used. Ordinary symbols denote scalar quantities in the main text, and vectors or matrices are shown in bold.

$\mathbb{R}$	space of real-valued
$\mathbb{C}$	space of complex-valued
Re	real part of a complex number
Im	imaginary part of a complex number
$[\cdot]^{\mathrm{T}}$	matrix transpose
$[\cdot]^{*}$	complex conjugate of a complex number
$\lvert\cdot\rvert$	magnitude a complex number
$\mathrm{Diag}(\cdot)$	operator of diagonalizing a vector

A. Single-Phase Feeder Model

The system is assumed to be a portion of a symmetric and balanced distribution network connected to the grid at one point, where the single-phase feeder model is adopted in [21].

Power Injection at Bus: Suppose a power distribution system with $n+1$ buses is collected in the set $\mathcal{N} \triangleq \{0, 1, \ldots, n\}$. The slack bus is located in bus 0, connected to the power grid delivering electricity to the following nodes. Modeling the other nodes in the network as the PQ buses, the power flow expression with complex power injections can be represented in matrix-vector form as

$$\boldsymbol{S}_{\boldsymbol{\mathcal{N}}} = \mathrm{diag}(\boldsymbol{V})\boldsymbol{I}^{*}, \tag{1}$$

where $\boldsymbol{V} = [V_1, ..V_i, ..V_n]^{\mathrm{T}}$ is the nodal voltage vector and $V_i = |V_i|\angle\theta_i \in \mathbb{C}$. $\boldsymbol{I} = [I_1, ..I_i, ..I_n]^{\mathrm{T}}$ is the nodal current vector, and $I_i \in \mathbb{C}$ denotes the current injected into bus i. With Kirchhoff's current law and slack bus voltage $V_0 \mathrm{e}^{\mathrm{j}\theta_0}$, the nodal current for all buses is presented as

$$\begin{bmatrix} I_0 \\ \boldsymbol{I} \end{bmatrix} = \begin{bmatrix} y & \overline{\boldsymbol{Y}}^{T} \\ \overline{\boldsymbol{Y}} & \boldsymbol{Y} \end{bmatrix} \begin{bmatrix} V_0 e^{j\theta_0} \\ \boldsymbol{V} \end{bmatrix}. \tag{2}$$

I_0 denotes the current injected into the slack bus. The dimensions of each block in the nodal admittance matrix are $\boldsymbol{Y} \in \mathbb{C}^{n\times n}$, $\overline{\boldsymbol{Y}} \in \mathbb{C}^{n}$, and $y \in \mathbb{C}$, respectively.

Power Flow in Branch: All branches in the power distribution system are contained in the set $\mathcal{L} \triangleq \{1, ..k, .., l\}$, where $k \in \mathcal{L}$ is represented by a set of two nodes as $k = \{i, j\}$. Let $\boldsymbol{I}_{\boldsymbol{\mathcal{L}}} = [I_1, ..I_k, ..I_l]^{\mathrm{T}}$, where $I_k \in \mathbb{C}$ denotes the line current in branch k. Then, the complex power flow of each line in $\mathcal{L}$ can be presented as

$$\boldsymbol{S}_{\boldsymbol{\mathcal{L}}} = \mathrm{diag}(\boldsymbol{V}_{\boldsymbol{\mathcal{L}}})\boldsymbol{I}^{*}_{\boldsymbol{\mathcal{L}}}, \tag{3}$$

where $\boldsymbol{V_{\mathcal{L}}} = [V_1, ..V_k, ..V_l]^{\mathrm{T}}$ is the branch voltage vector with entries $V_k = V_i \in \mathbb{C}$ for $k = \{i, j\}$. For the same structural expression as (2), the branch current and voltage relationship is represented as

$$\boldsymbol{I_{\mathcal{L}}} = \left[\begin{array}{cc} \boldsymbol{Y_{\mathcal{L}0}} & \boldsymbol{Y_{\mathcal{LN}}} \end{array} \right] \left[\begin{array}{c} V_0 e^{j\theta_0} \\ \boldsymbol{V} \end{array} \right], \tag{4}$$

where blocks $\boldsymbol{Y_{\mathcal{L}0}} \in \mathbb{C}^{l\times 1}$ and $\boldsymbol{Y_{\mathcal{LN}}} \in \mathbb{C}^{l\times n}$ combining into the branch admittance matrix.

B. FASE Model

Under normal operating conditions, the power system is generally maintained in quasi-steady states. In other words, the system state experiences a gradual change due to smooth and slow bus power variations. To perceive this changing process, the model building of FASE delves into the dynamic evolution of static system state by combining real-time measurements. The dynamic state-space model of FASE is represented in the following discrete form:

$$\boldsymbol{x}_{k+1} = \boldsymbol{F}_k \boldsymbol{x}_k + \boldsymbol{g}_k + \boldsymbol{w}_k, \tag{5}$$

$$\boldsymbol{z}_k = \boldsymbol{h}_k(\boldsymbol{x}_k) + \boldsymbol{v}_k, \tag{6}$$

where k is the time sample; $\boldsymbol{x}_k$ represents the system state vector, $\boldsymbol{F}_k$ is the state transition matrix; $\boldsymbol{g}_k$ is the trend behavior vector of the state trajectory; $\boldsymbol{z}_k$ is the measurement vector; functions $\boldsymbol{h}_k(\cdot)$ give the nonlinear measurement relationship between state variables and meters; $\boldsymbol{w}_k$ is a Gaussian process noise vector with zero mean and $\boldsymbol{Q_{w,k}}$ covariance; $\boldsymbol{v}_k$ is a Gaussian measurement error vector with zero mean and $\boldsymbol{R_{v,k}}$ covariance, and worthy noting that uncertainties factors $\boldsymbol{w}_k$ and $\boldsymbol{v}_k$ are assumed to be uncorrelated.

As mentioned in introduction, time series analysis models [16], [24]–[26] have been widely used to interpret the state forecasting process in (5) with time evolution. However, manually selecting $\boldsymbol{F}_k$ and $\boldsymbol{g}_k$ based on prior experience becomes a tough task, as parameters need to be statistically estimated to account for specific scenarios following extensive simulations. In (6), the measurement functions $\boldsymbol{h}_k(\cdot)$ typically represent the standard real and reactive power observation of node power injection or line power flow. With the advancement of PMU technology, direct measuring states of voltage magnitude and phase angle are also possible [27], [28]. However, the extensive collection of real-time observations may not only raise meter installation costs but also lead to filtering information redundancy.

III. Static Approximations to System States

With a voltage perturbation vector around the nominal value replacing the overall depiction of the nodal voltage state, we first propose the linear approximations of power flow solutions based on power injection and power flow measurements. Then, the static approximate system states are obtained from a single scan of measurements.

A. Approximating State From Power Injection Measurements

The complex power injections in (1) can be succinctly expressed using (2),

$$\begin{aligned} \boldsymbol{S_{\mathcal{N}}} &= \mathrm{diag}(\boldsymbol{V})\boldsymbol{I}^* \\ &= \mathrm{diag}(\boldsymbol{V})\left(\boldsymbol{Y}^*\boldsymbol{V}^* + \overline{\boldsymbol{Y}}^* V_0 \mathrm{e}^{-\mathrm{j}\theta_0}\right). \end{aligned} \tag{7}$$

For effectively deriving voltage states in the power-balance expression of (7), an optimal solution is assumed by $\boldsymbol{V}^\star \in \mathbb{C}^n$, consisting of the priori-determined nominal voltage vector $\boldsymbol{V_n}$ and a perturbation vector $\boldsymbol{\Delta V}$, i,e., $\boldsymbol{V}^\star = \boldsymbol{V_n} + \boldsymbol{\Delta V}$.

Substituting $\boldsymbol{V}^\star$ into (7) and expanding the terms, $\boldsymbol{S_{\mathcal{N}}}$ is expressed with $\boldsymbol{V_n}$ and $\boldsymbol{\Delta V}$ as

$$\begin{aligned} \boldsymbol{S_{\mathcal{N}}} &= \mathrm{diag}(\boldsymbol{V}^\star)(\boldsymbol{Y}^*(\boldsymbol{V}^\star)^* + \overline{\boldsymbol{Y}}^* V_0 \mathrm{e}^{-\mathrm{j}\theta_0}) \\ &= \mathrm{diag}(\boldsymbol{V_n} + \boldsymbol{\Delta V})(\boldsymbol{Y}^*(\boldsymbol{V_n} + \boldsymbol{\Delta V})^* + \overline{\boldsymbol{Y}}^* V_0 \mathrm{e}^{-\mathrm{j}\theta_0}) \\ &= \mathrm{diag}(\boldsymbol{V_n})(\boldsymbol{Y}^*\boldsymbol{V_n}^* + \overline{\boldsymbol{Y}}^* V_0 \mathrm{e}^{-\mathrm{j}\theta_0}) \\ &+ \mathrm{diag}(\boldsymbol{\Delta V})\boldsymbol{Y}^*\boldsymbol{V_n}^* + \mathrm{diag}(\boldsymbol{\Delta V})\boldsymbol{Y}^*\boldsymbol{\Delta V}^* \\ &+ \mathrm{diag}(\boldsymbol{\Delta V})\overline{\boldsymbol{Y}}^* V_0 \mathrm{e}^{-\mathrm{j}\theta_0} + \mathrm{diag}(\boldsymbol{V_n})\boldsymbol{Y}^*\boldsymbol{\Delta V}^*. \end{aligned} \tag{8}$$

From the above formulas, we can recognize that

$$\mathrm{diag}(\boldsymbol{\Delta V})\boldsymbol{Y}^*\boldsymbol{V_n}^* = \mathrm{diag}(\boldsymbol{Y}^*\boldsymbol{V_n}^*)\boldsymbol{\Delta V},$$
$$\mathrm{diag}(\boldsymbol{\Delta V})\boldsymbol{Y}^*\boldsymbol{\Delta V}^* = \mathrm{diag}(\boldsymbol{Y}^*\boldsymbol{\Delta V}^*)\boldsymbol{\Delta V},$$
$$\mathrm{diag}(\boldsymbol{\Delta V})\overline{\boldsymbol{Y}}^* V_0 \mathrm{e}^{-\mathrm{j}\theta_0} = V_0 \mathrm{e}^{-\mathrm{j}\theta_0}\ \mathrm{diag}(\overline{\boldsymbol{Y}}^*)\boldsymbol{\Delta V}.$$

Then, (9) is reorganized as

$$\begin{aligned} \boldsymbol{S_{\mathcal{N}}} &= \mathrm{diag}(\boldsymbol{V_n})(\boldsymbol{Y}^*\boldsymbol{V_n}^* + \overline{\boldsymbol{Y}}^* V_0 \mathrm{e}^{-\mathrm{j}\theta_0}) \\ &+ \big(\mathrm{diag}(\boldsymbol{Y}^*\boldsymbol{V_n}^*) + \mathrm{diag}(\boldsymbol{Y}^*\boldsymbol{\Delta V}^*) \\ &+ V_0 \mathrm{e}^{-\mathrm{j}\theta_0}\ \mathrm{diag}(\overline{\boldsymbol{Y}}^*)\big)\boldsymbol{\Delta V} + \mathrm{diag}(\boldsymbol{V_n})\boldsymbol{Y}^*\boldsymbol{\Delta V}^*. \end{aligned} \tag{9}$$

Based on structure expression of (9), the nominal voltage vector $\boldsymbol{V_n}$ can be customized as

$$\boldsymbol{V_n} = -\boldsymbol{Y}^{-1}\overline{\boldsymbol{Y}} V_0 \mathrm{e}^{\mathrm{j}\theta_0}, \tag{10}$$

where $\boldsymbol{Y} \in \mathbb{C}^{\boldsymbol{n}\times\boldsymbol{n}}$ is invertible. $\boldsymbol{V_n}$ in (10) is also the non-zero solution to (7) when $\boldsymbol{S_{\mathcal{N}}} = \boldsymbol{0}$, and now the current injections at buses are zeros. It can be referred to as the no-load voltage in power distribution systems [29]. And consider $\boldsymbol{Y}$ and $\overline{\boldsymbol{Y}}$ in the nodal admittance matrix satisfying

$$\boldsymbol{Y}^{-1}\overline{\boldsymbol{Y}} = -\boldsymbol{1}, \tag{11}$$

where $\boldsymbol{1}$ is the vector of all ones. Substituting (10) into (9), we can get

$$\boldsymbol{S_{\mathcal{N}}} = \mathrm{diag}(\boldsymbol{Y}^*\boldsymbol{\Delta V}^*)\boldsymbol{\Delta V} + \mathrm{diag}(\boldsymbol{V_n})\boldsymbol{Y}^*\boldsymbol{\Delta V}^*. \tag{12}$$

Neglecting the intractable quadratic term of $\boldsymbol{\Delta V}$ for linear analysis, the approximate voltage perturbation vector based on power injection measurements is obtained as

$$\boldsymbol{\Delta V} \approx \boldsymbol{Y}^{-1}\,\mathrm{diag}(1/V_0 \mathrm{e}^{-\mathrm{j}\theta_0}\boldsymbol{1})\boldsymbol{S}^*_{\boldsymbol{\mathcal{N}}}. \tag{13}$$

Then, using (10) and (13), the following remark is made.

Remark 1: Based on the power injection measurements, the optimal voltage state vector is approximated as

$$\begin{aligned} \boldsymbol{V}^* &= \boldsymbol{V_n} + \boldsymbol{\Delta V} \\ &\approx V_0 \mathrm{e}^{\mathrm{j}\theta_0}\boldsymbol{1} + \boldsymbol{Y}^{-1}\,\mathrm{diag}(1/V_0 \mathrm{e}^{-\mathrm{j}\theta_0}\boldsymbol{1})\boldsymbol{S}^*_{\boldsymbol{\mathcal{N}}}. \end{aligned} \tag{14}$$

B. Approximating State From Power Flow Measurements

The complex power flows in (3) can be succinctly expressed using (4), while substituting the assumed optimal solution $\boldsymbol{V}^{\star}$,

$$\begin{aligned}\boldsymbol{S}_{\boldsymbol{\mathcal{L}}} &= \operatorname{diag}(\boldsymbol{V}_{\boldsymbol{\mathcal{L}}})\boldsymbol{I}_{\boldsymbol{\mathcal{L}}}^{*} \\ &= \operatorname{diag}(\boldsymbol{V}_{\boldsymbol{\mathcal{L}}})\left(\boldsymbol{Y}_{\boldsymbol{\mathcal{L}0}}^{*}V_0e^{-j\theta_0} + \boldsymbol{Y}_{\boldsymbol{\mathcal{L}\mathcal{N}}}^{*}(\boldsymbol{V_n}+\boldsymbol{\Delta V})^{*}\right).\end{aligned} \tag{15}$$

With the same choice of $\boldsymbol{V_n} = V_0e^{j\theta_0}\mathbf{1}$ in (10) and rearranging the terms in (15), we can get

$$\boldsymbol{\Delta V} = \boldsymbol{Y}_{\boldsymbol{\mathcal{L}\mathcal{N}}}^{-1}\operatorname{diag}(1/\boldsymbol{V}_{\boldsymbol{\mathcal{L}}}^{*})\boldsymbol{S}_{\boldsymbol{\mathcal{L}}}^{*} - \boldsymbol{Y}_{\boldsymbol{\mathcal{L}\mathcal{N}}}^{-1}\boldsymbol{Y}_{\boldsymbol{\mathcal{L}0}}V_0e^{j\theta_0} - \boldsymbol{V_n}. \tag{16}$$

In literature on operation and control of power distribution networks, simple analyses are often performed for power lines, assuming a minor difference in voltage amplitude or phase angle between two nodes [18], [19], [30]. That is, we set the voltage at the beginning of each line equal to $V_0e^{j\theta_0}$, i.e., $\boldsymbol{V_{\mathcal{L}}} = \boldsymbol{V_n}$. Simultaneously, consider $\boldsymbol{Y_{\mathcal{L}0}}$ and $\boldsymbol{Y_{\mathcal{L}\mathcal{N}}}$ in the branch admittance matrix satisfying

$$\boldsymbol{Y}_{\boldsymbol{\mathcal{L}\mathcal{N}}}^{-1}\boldsymbol{Y}_{\boldsymbol{\mathcal{L}0}} = -\mathbf{1}. \tag{17}$$

Rearranging the terms in (16), the approximate voltage perturbation vector based on power flow measurements is obtained as

$$\boldsymbol{\Delta V} \approx \boldsymbol{Y}_{\boldsymbol{\mathcal{L}\mathcal{N}}}^{-1}\operatorname{diag}(1/V_0e^{-j\theta_0}\mathbf{1})\boldsymbol{S}_{\boldsymbol{\mathcal{L}}}^{*}, \tag{18}$$

where the pseudo-inverse operation is performed on admittance matrix $\boldsymbol{Y_{\mathcal{L}\mathcal{N}}} \in \mathbb{C}^{l\times n}$.

Then, using (10) and (18), the following remark is made.

Remark 2: Based on the power flow measurements, the optimal voltage state vector is approximated as

$$\begin{aligned}\boldsymbol{V}^{*} &= \boldsymbol{V_n} + \boldsymbol{\Delta V} \\ &\approx V_0\mathrm{e}^{\mathrm{j}\theta_0}\mathbf{1} + \boldsymbol{Y}_{\boldsymbol{\mathcal{L}\mathcal{N}}}^{-1}\operatorname{diag}(1/V_0e^{-j\theta_0}\mathbf{1})\boldsymbol{S}_{\boldsymbol{\mathcal{L}}}^{*}.\end{aligned} \tag{19}$$

To summarize the preceding, static approximate states (14) and (19) explicitly present linear approximations of the power flow solutions, i.e., nodal voltage states, from power injection and power flow measurements.

IV. Dynamic Approximations to FASE

Based on *Remark 1* and *2* in Section III, the linear approximations are introduced into the dynamic FASE framework. For state forecasting, we derive the system state prediction model with only nodal impedance parameters from the approximate model based on power injection measurements. In the filtering process, the observation equation is from the approximation based on power flow measurements, where an observation matrix composed of branch admittance parameters is constructed.

A. State Forecasting

Considering the dynamic elements, power variations in load and DG buses are defined as the trend behavior vector in (5), driving the transition of the voltage state. Hence, a full system state $\boldsymbol{\Xi} = [\boldsymbol{\Delta V}^T \ \ \boldsymbol{S}_{\boldsymbol{\mathcal{N}}}^T]^T$ can be jointly explored including the nodal voltage perturbation vector and power injections. Based on the approximate power balance expression in (13), the full derivation on the full system state indicates as follows:

$$d\boldsymbol{\Delta V} = \boldsymbol{Y}^{-1}\operatorname{diag}(1/V_0\mathrm{e}^{-\mathrm{j}\theta_0}\mathbf{1})d\boldsymbol{S}_{\boldsymbol{\mathcal{N}}}^{*}, \tag{20}$$

where the perturbation vector replaces complete voltage profile and is represented as the algebraic state $\boldsymbol{x}$ in (5). The injected power variations at system nodes act as a driver, influencing the trend behavior of the perturbation vector, as defined by $\boldsymbol{g}$ in (5).

In rectangular coordinates, the perturbation vector is succinctly expressed as $\boldsymbol{\Delta V} = \boldsymbol{\Delta V_{\mathrm{Re}}} + j\boldsymbol{\Delta V_{\mathrm{Im}}}$, where $\boldsymbol{\Delta V_{\mathrm{Re}}}$ and $\boldsymbol{\Delta V_{\mathrm{Im}}} \in \mathbb{R}^n$ represent the real and imaginary components of $\boldsymbol{\Delta V}$, respectively. Denote the inverse of nodal admittance matrix by impedance matrix, i.e., $\boldsymbol{Y}^{-1} = (\boldsymbol{R}+j\boldsymbol{X})$. With the choice of $V_0 = 1$ p.u. and $\theta_0 = 0^{\circ}$ for the slack bus voltage, and $\boldsymbol{S_{\mathcal{N}}} = \boldsymbol{P} + j\boldsymbol{Q}$, (20) is reorganized in rectangular form to get

$$d(\boldsymbol{\Delta V_{\mathrm{Re}}} + j\boldsymbol{\Delta V_{\mathrm{Im}}}) = (\boldsymbol{R}+j\boldsymbol{X})d(\boldsymbol{P}-j\boldsymbol{Q}). \tag{21}$$

Expanding and rearranging the terms in (21), the derivations on real and imaginary components of $\boldsymbol{\Delta V}$ are obtained as

$$\begin{bmatrix} d\boldsymbol{\Delta V_{\mathrm{Re}}} \\ d\boldsymbol{\Delta V_{\mathrm{Im}}} \end{bmatrix} = \begin{bmatrix} \boldsymbol{R} & \boldsymbol{X} \\ \boldsymbol{X} & -\boldsymbol{R} \end{bmatrix}\begin{bmatrix} d\boldsymbol{P} \\ d\boldsymbol{Q} \end{bmatrix}. \tag{22}$$

Therefore, for two adjacent operating points in a short time interval, the state transition process is derived from (22) as

$$\begin{bmatrix} \boldsymbol{\Delta V_{\mathrm{Re}}} \\ \boldsymbol{\Delta V_{\mathrm{Im}}} \end{bmatrix}_{k+1} = \begin{bmatrix} \boldsymbol{\Delta V_{\mathrm{Re}}} \\ \boldsymbol{\Delta V_{\mathrm{Im}}} \end{bmatrix}_{k} + \begin{bmatrix} \boldsymbol{R} & \boldsymbol{X} \\ \boldsymbol{X} & -\boldsymbol{R} \end{bmatrix}\begin{bmatrix} d\boldsymbol{P} \\ d\boldsymbol{Q} \end{bmatrix}_{k} + \boldsymbol{w_k}, \tag{23}$$

where $\boldsymbol{w_k}$ becomes the linearization error between two operation points as process noise. And the dynamic algebraic state is $\boldsymbol{x} = [\boldsymbol{\Delta V}_{\mathbf{Re}}^T \ \ \boldsymbol{\Delta V}_{\mathbf{Im}}^T]^T \in \mathbb{R}^{2n\times 1}$. The active and reactive power variations are denoted by $d\boldsymbol{S_{\mathcal{N}}} = [d\boldsymbol{P}^T \ d\boldsymbol{Q}^T]^T \in \mathbb{R}^{2m\times 1}$. Based on the structure of Kalman filtering and (23), a priori forecasted state $\tilde{\boldsymbol{x}}_{k+1}$ and its error covariance matrix $\boldsymbol{M}_{k+1}$ will be obtained from last time sample k as

$$\tilde{\boldsymbol{x}}_{k+1} = \hat{\boldsymbol{x}}_k + \boldsymbol{T}d\boldsymbol{S_{\mathcal{N}}}, \tag{24}$$

$$\boldsymbol{M}_{k+1} = \boldsymbol{\Sigma}_k + \boldsymbol{Q}_{w,k}, \tag{25}$$

where

$$\boldsymbol{T} = \begin{bmatrix} \boldsymbol{R} & \boldsymbol{X} \\ \boldsymbol{X} & -\boldsymbol{R} \end{bmatrix}. \tag{26}$$

$\hat{\boldsymbol{x}}_k$ is from the optimal estimate (a posteriori estimate) at time sample k with its covariance matrix $\boldsymbol{\Sigma}_k$, and the constant matrix $\boldsymbol{T}$ consists of the nodal resistance and reactance block entries.

Remark 3: Based on information of the nodal impedance components $\boldsymbol{R}$ and $\boldsymbol{X}$, the real and imaginary parts of $\boldsymbol{\Delta V}$ can be predicted as stated in (24), with the updating of priori error covariance matrix $\boldsymbol{M}_{k+1}$ in (25).

B. State Filtering

Determining an efficient observation equation is essential to the state filtering process. Regardless of the measurement type, power flow models always run through the functional dependency between real-time measures and state variables. In this paper, we utilize the approximate power flow model in (18) to execute the state update step:

$$\boldsymbol{S}_{\boldsymbol{\mathcal{L}}}^{*} = \operatorname{diag}(V_0\mathrm{e}^{-\mathrm{j}\theta_0})\boldsymbol{Y_{\mathcal{L}\mathcal{N}}}\boldsymbol{\Delta V}, \tag{27}$$

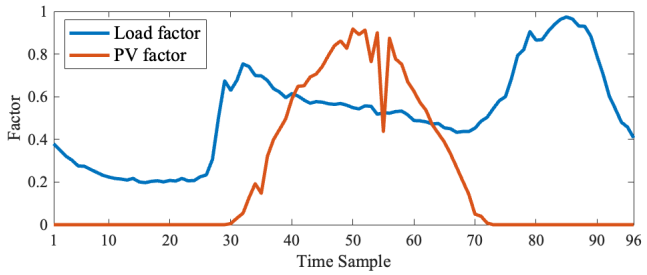

Fig. 1. Forecasted PV factor and load factor profiles.

where $\boldsymbol{Y}_{\mathcal{LN}} = \boldsymbol{G}_{\mathcal{L}} + j\boldsymbol{B}_{\mathcal{L}}$ represents the branch admittance matrix, and $\boldsymbol{S}_{\mathcal{L}} = \boldsymbol{P}_{\mathcal{L}} + j\boldsymbol{Q}_{\mathcal{L}}$. Consistent with the expression of $\boldsymbol{\Delta V}$ and parameter settings of slack bus in state forecasting, the approximate measurement function based on (27) is built as

$$\begin{bmatrix} \boldsymbol{P}_{\mathcal{L}} \\ \boldsymbol{Q}_{\mathcal{L}} \end{bmatrix}_k = \begin{bmatrix} \boldsymbol{G}_{\mathcal{L}} & -\boldsymbol{B}_{\mathcal{L}} \\ -\boldsymbol{B}_{\mathcal{L}} & -\boldsymbol{G}_{\mathcal{L}} \end{bmatrix} \begin{bmatrix} \boldsymbol{\Delta V}_{\mathbf{Re}} \\ \boldsymbol{\Delta V}_{\mathbf{Im}} \end{bmatrix}_k + \boldsymbol{v}_k, \quad (28)$$

where the measurement vector is $\boldsymbol{z}_k = [\boldsymbol{P}_{\mathcal{L}}^T \ \boldsymbol{Q}_{\mathcal{L}}^T]^T \in \mathbb{R}^{2l\times 1}$. The active and reactive branch flow measurements are included along with their corresponding noises vector $\boldsymbol{v}_k$. The linear approximate mapping relationship between branch flow measurements and states is embodied by the constant observation matrix $\boldsymbol{H}$, given as

$$\boldsymbol{H} = \begin{bmatrix} \boldsymbol{G}_{\mathcal{L}} & -\boldsymbol{B}_{\mathcal{L}} \\ -\boldsymbol{B}_{\mathcal{L}} & -\boldsymbol{G}_{\mathcal{L}} \end{bmatrix}. \quad (29)$$

Then, the updated $\hat{\boldsymbol{x}}_{k+1}$ is computed:

$$\hat{\boldsymbol{x}}_{k+1} = \tilde{\boldsymbol{x}}_{k+1} + \boldsymbol{K}_{k+1}(\boldsymbol{z}_{k+1} - \tilde{\boldsymbol{z}}_{k+1}), \quad (30)$$

where

$$\boldsymbol{K}_{k+1} = \boldsymbol{M}_{k+1}\boldsymbol{H}^T(\boldsymbol{H}\boldsymbol{M}_{k+1}\boldsymbol{H}^T + \boldsymbol{R}_{v,k+1})^{-1}, \quad (31)$$

$$\tilde{\boldsymbol{z}}_{k+1} = \boldsymbol{H}\tilde{\boldsymbol{x}}_{k+1}. \quad (32)$$

The posterior covariance matrix $\boldsymbol{\Sigma}_{k+1}$ is updated as

$$\boldsymbol{\Sigma}_{k+1} = (\boldsymbol{I} - \boldsymbol{K}_{k+1}\boldsymbol{H})\boldsymbol{M}_{k+1}. \quad (33)$$

Remark 4: Based on information of the branch admittance components $\boldsymbol{G}_{\mathcal{L}}$ and $\boldsymbol{B}_{\mathcal{L}}$, the real and imaginary parts of $\boldsymbol{\Delta V}$ can be updated as stated in (30), with the updating of posterior error covariance matrix $\boldsymbol{\Sigma}_{k+1}$ in (33).

In summary, the optimal estimation of the voltage perturbation vector $\boldsymbol{\Delta V}$ is approximated by the APF-FASE estimator. Furtherly, combined with the priori determined nominal vector $\boldsymbol{V_n}$, dynamic voltage states are entirely depicted. Throughout the proposed estimator, it is necessary to consider the uncertainty of injected power variations $\boldsymbol{S}_{\mathcal{N}}$ between adjacent time instants, which has been included in simulations. Powerful forecasting tools on load and DG variations, which are not the focus of this paper but can be referenced for further information, are available in the published literature [31]–[33].

TABLE I
STATE PREDICTION AND FILTERING CONFIGURATION FOR THE SIX ESTIMATORS

Method \ Stage	State Forecasting	State Filtering
DC-FASE-I	Holt's method	θ, DC PJ and PF
EKF-FASE-I		$\lvert V\rvert$, Nonlinear PJ and PF
APF-FASE-I		$\lvert V\rvert$, Remark 1 and 2
DC-FASE-II	d(DC PJ)/d(x, S_N)	θ, DC PF
EKF-FASE-II	d(Nonlinear PJ)/d(x, S_N)	$\lvert V\rvert$, Nonlinear PF
APF-FASE-II	Remark 3	$\lvert V\rvert$, Remark 4

V. SIMULATION RESULTS

To validate the proposed FASE method in previous sections, a symmetric balanced 56-node power distribution system [18], modified from the IEEE 123-node test feeder, is adopted for testing. Suppose that a grid connected PV system with a rated power of 150kWp is located at bus 15. The system states are dynamically estimated every 15 minutes following the PV and load variations. The PV and load data are provided by multiplying forecasted PV and load factors, as illustrated in Fig. 1, with the peak PV capacity and the peak load, respectively, while adding a random fluctuation with a linear trend (1%-3%). In total, 96 dynamic processes throughout one day are included. All simulations are performed on a standard commercial notebook equipped with an Intel i5 core at 1.7 GHz and 8 GB RAM, running the Matlab environment.

A. Performance Comparisons

The efficiency and robustness of nonlinear and linear power flow model-based FASE estimators are included in comparisons under different simulation scenarios. Different state forecasting and filtering configurations for the six estimators are shown in Table I, where $|V|$ and θ represents the measurement of voltage magnitude and phase angle; nonlinear PJ and PF represents the nonlinear measurement equations of power injection and power flow in filtering stage (i.e., extended Kalman filter, EKF [28]). For EKF-FASE-II and DC-FASE-II, the full system state derivation on the nonlinear PJ and DC PJ equations are implemented as the state transition model in forecasting stage. Different combinations of settings demonstrate the performance of the proposed APF-FASE estimator on using voltage perturbation as the state variable, utilizing power injection variations in the prediction stage, and linearizing power flow equations in the filtering stage.

For the classical Holt's linear method, validation parameters in [28] are used, which set $\boldsymbol{a_0} = \boldsymbol{x_0}$, $\boldsymbol{b_0} = \boldsymbol{0}$, and the two fractional parameters set $\alpha_t = 0.8$, $\beta_t = 0.5$. The state noise covariance matrix is $\boldsymbol{Q}_{w,k} = \mathrm{diag}(\boldsymbol{Q}_V, \boldsymbol{Q}_\theta)$. The larger noise $\boldsymbol{Q}_\theta = (4\times 10^{-4})\boldsymbol{I}$ is set for phase angle compared to the $\boldsymbol{Q}_V = (10^{-4})\boldsymbol{I}$ for voltage magnitude, where more nonlinearity is induced by phase angle to highlight specific advantages of the APF-FASE. The standard deviation σ_i in measurement noises matrix $\boldsymbol{R}_{v,k}$ can be assumed as $\sigma_i = (0.02a + 0.0052f_s)/3$, where a is the measured value and f_s is the full scale value of instrumentation [19]. In this paper, the standard deviation of measurement noise in power injection,

TABLE II
COMPARISON OF MAE FOR VOLTAGE MAGNITUDE AND PHASE ANGLE IN STATE FORECASTING AND FILTERING

Method \ Stage	State Forecasting		State Filtering	
	$\lvert\tilde{V}\rvert$ $(p.u.)$	$\angle\tilde{\theta}$ $(^\circ)$	$\lvert\hat{V}\rvert$ $(p.u.)$	$\angle\hat{\theta}$ $(^\circ)$
DC-FASE-I	-	0.3619	-	0.3380
EKF-FASE-I	0.0024	0.1116	1.30E-4	0.0064
APF-FASE-I	0.0023	0.1079	4.17E-4	8.44E-4
DC-FASE-II	-	0.3388	-	0.3380
EKF-FASE-II	0.0017	0.1378	1.79E-5	1.44E-3
APF-FASE-II	4.16E-4	0.0010	4.10E-4	8.43E-4

TABLE III
COMPARISON OF MRE FOR VOLTAGE MAGNITUDE AND PHASE ANGLE IN STATE FORECASTING AND FILTERING

Method \ Stage	State Forecasting		State Filtering	
	$\lvert\tilde{V}\rvert$ $(p.u.)$	$\angle\tilde{\theta}$ $(^\circ)$	$\lvert\hat{V}\rvert$ $(p.u.)$	$\angle\hat{\theta}$ $(^\circ)$
DC-FASE-I	-	81.80%	-	75.64%
EKF-FASE-I	12.04%	27.24%	0.73%	1.43%
APF-FASE-I	10.90%	21.33%	1.36%	0.27%
DC-FASE-II	-	76.21%	-	76.10%
EKF-FASE-II	8.41%	42.25%	0.08%	0.31%
APF-FASE-II	1.36%	0.38%	1.34%	0.34%

power flow and voltage magnitude is 0.01, 0.008 and 0.03, respectively. For all estimators, voltage magnitude measurements are also integrated at the node set $\{1, 9, 16, 26, 32, 36, 39, 46\}$, and setting of $V_0 = 1$ p.u. and $\theta_0 = 0^\circ$ for the slack bus voltage. Use PV and load data as input to power flow analysis to get true system states. And the power flow measurements are derived from the successful power flow calculation while adding random Gaussian noise (zero mean and 1% standard deviations). Four scenarios primarily associated with FASE applications are consider to investigate estimators performance:

- *Normal conditions*: The power system operates under a quasi-stationary regime that experiences changes caused by smooth, slow load and DG variations.
- *Limited real-time measurements*: Different numbers of power injection and power flow measurements are configured, with redundancy ranging from 1.2 to 1.8.
- *Sudden state changes*: In state forecasting, unpredictable sudden changes can occur in power injections, such as an abrupt increase in a load bus.
- *Occurrence of outliers*: In state filtering, false data can be injected into measurements, such as stealthily tampered by cyber-attacks.

The averaged results over 100 independent experiments are statistical on the state forecasting and filtering process by the following two metrics:

1) MAE: The mean-absolute-error of forecasted and filtered voltage magnitude and phase angle. Take the forecasted voltage magnitude $|\tilde{\boldsymbol{V}}|$ as an illustration,

$$|\tilde{\boldsymbol{V}}|_{\text{MAE}} = \frac{1}{N_{DC}} \sum_{j=1}^{N_{DC}} \frac{1}{n} \sum_{i=1}^{n} \left| |\tilde{V}_i| - |V_i| \right|. \tag{34}$$

2) MRE: The mean-relative-error of forecasted or filtered voltage magnitude and phase angle. Take the forecasted voltage magnitude $|\tilde{\boldsymbol{V}}|$ as an illustration,

$$|\tilde{\boldsymbol{V}}|_{\text{MRE}} = \frac{1}{N_{DC}} \sum_{j=1}^{N_{DC}} \frac{1}{n} \sum_{i=1}^{n} \left| |\tilde{V}_i| - |V_i| \right| / \left| |V_0| - |V_i| \right|. \tag{35}$$

In above formulas, V_i and $\tilde{V}_i$ represent the true and forecasted voltage state at bus i, respectively. N_{DC} is the total number of dynamic change times. And the corresponding metric for filtered state is presented by substituting $\hat{\boldsymbol{V}}$ for $\tilde{\boldsymbol{V}}$.

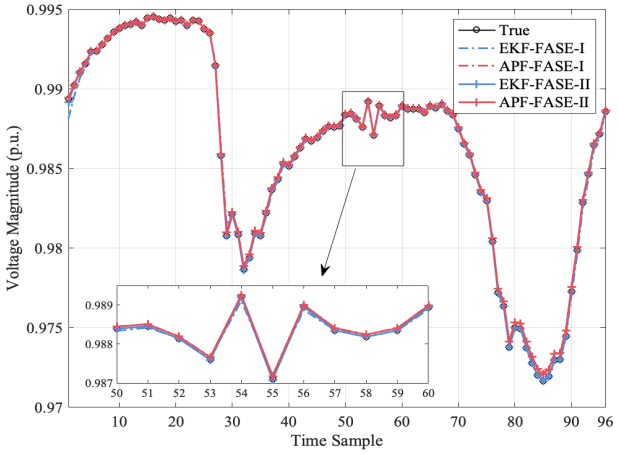

(a) Voltage Magnitude

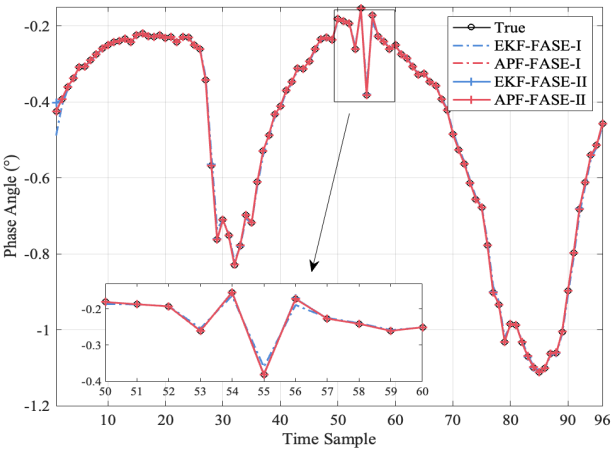

(b) Phase Angle

Fig. 2. Comparison results of estimating voltage magnitude and phase angle at bus 4 in the 56-node test system. (a) Voltage Magnitude. (b) Phase Angle.

B. Results and Discussion

1) Normal Conditions: Smooth and slow load variations are considered in this case with normal measurements. With a complete measurement configuration, i.e., power injection and power flow measurement are available in each bus and branch, the statistical MAE and MRE of the forecasted and filtered voltage states for all estimators are listed in Table II-III. Due to the approximation assumption that all voltage magnitudes are at 1 p.u. in DC power flow model, only the phase angle results of DC-FASE-I and II are considered as the reference

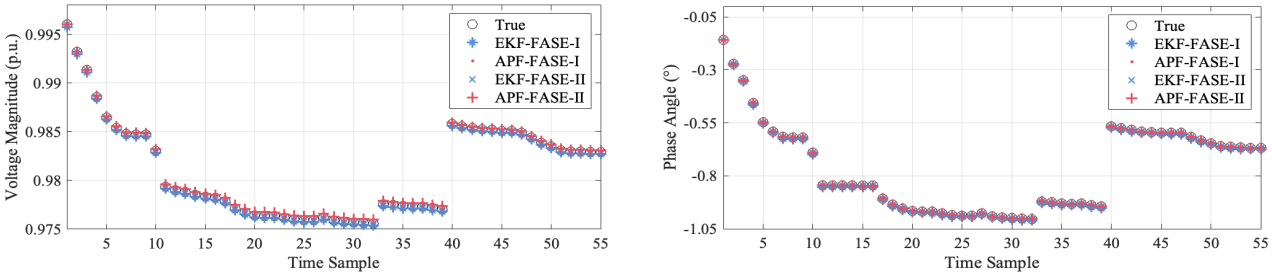

(a) Voltage Magnitude (b) Phase Angle

Fig. 3. Comparison of estimated states for all buses at final time sample. (a) Voltage Magnitude. (b) Phase Angle.

TABLE IV
DIFFERENT MEASUREMENT CONFIGURATIONS FOR TEST SYSTEM

Redundancy	NoV[1,2]	NoPJ [3]	NoPF
1.2	8	52	72
1.4	8	60	86
1.6	8	72	96
1.8	8	84	106

[1] NoV: Number of voltage measurements; NoPJ: Number of power injection measurements; NoPF: Number of power flow measurements.
[2] Tests without voltage measurements for APF-FASE-II.
[3] Forecasted power injection pseudo-measurements are limited in state forecasting stage of EKF-FASE-II and APF-FASE-II.

benchmark for linearization techniques.

Using the classical Holt's linear method as state prediction model, the APF-FASE-I that defines the voltage perturbation vector as state variable can provide more refined depiction of the voltage state changes and obtain more accurate prediction results than EKF-FASE-I and DC-FASE-I. Meanwhile, the approximate measurement equations in APF-FASE-I (*Remark 1* and *Remark 2*) sustain superior filtering capability against the nonlinear observation of phase angles in EKF-FASE-I, and comparable estimation results on voltage magnitudes are obtained. For power injection model-based state forecasting, the approximate state transition model (*Remark 3*) in APF-FASE-II efficiently presents the state change process accompanying the power injection variations, where the accurate forecasting performance contribute to reducing filtering difficulty.

Note that, the filtering results of APF-FASE-II keep pace with APF-FASE-I, where the filtering process is only based on the proposed approximate power flow model (*Remark 4*) and magnitude measurements. Although the EKF-FASE-II demonstrates the optimal filtering results by utilizing comprehensive power flow equations, the APF-FASE-II relying on the linear approximations closely trails. For example, the voltage fluctuations of bus 4 for all estimators are shown in Fig. 2. The comparison of the estimated states at the final step for all buses is presented in Fig. 3. It is intuitive to see that all estimators closely track the trajectory of voltage changes, whether in terms of the voltage magnitude or phase angle. However, the APF-FASE-II attains unique advantages, such as explicit parameter presetting for state transition model and the absence of computational complexity associated with the measurement Jacobian matrix.

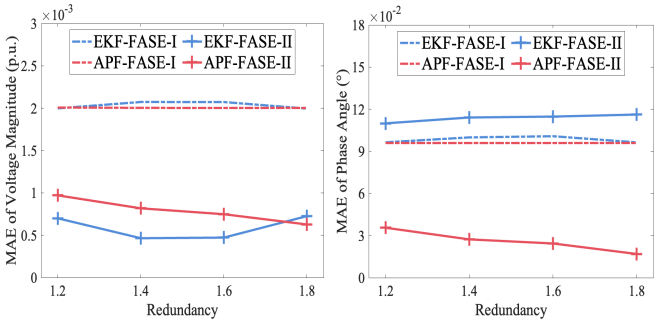

(a) Voltage Magnitude (b) Phase Angle

Fig. 4. MAE curves for forecasted states with limited real-time measurements. (a) Voltage Magnitude. (b) Phase Angle.

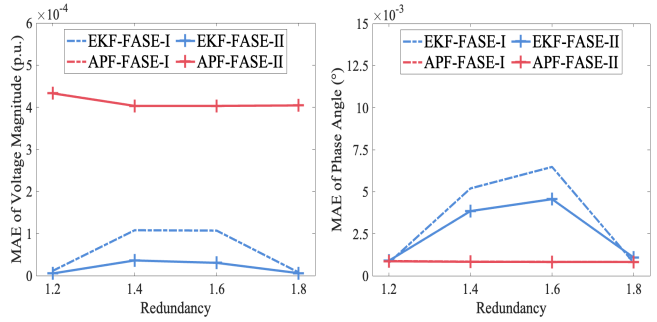

(a) Voltage Magnitude (b) Phase Angle

Fig. 5. MAE curves for filtered states with limited real-time measurements. (a) Voltage Magnitude. (b) Phase Angle.

2) Limited Real-time Measurements: In actual power systems, the real-time measuring availability is subject to time-varying and installation conditions, which directly decide the observability of the system state and whether it can be timely estimated. Therefor, simulations with different measurement redundancies ranging from 1.2 to 1.8 are performed between estimators, where the specific configuration is shown in Table IV. For the EKF-FASE-I and APF-FASE-I, both power injection and power flow real-time measurements in filtering stage are limited. Especially for the EKF-FASE-II and APF-FASE-II, the availability of forecasted power variations is limited during the state forecasting, and the real-time power flow measurements are limited in state filtering. Furthermore,

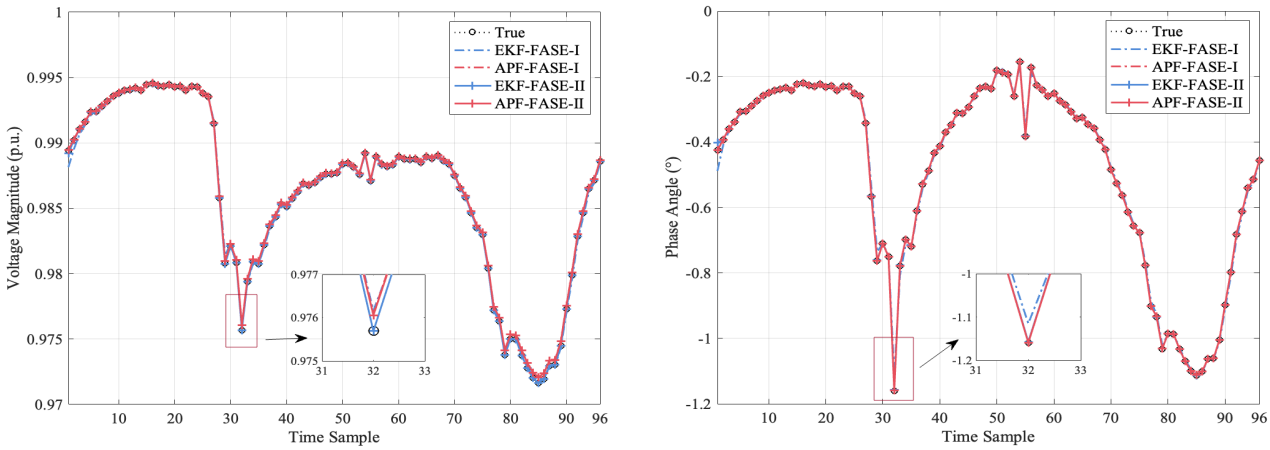

(a) Voltage Magnitude (b) Phase Angle

Fig. 6. Comparison results of estimating voltage magnitude and phase angle at bus 4 with sudden load happens. (a) Voltage Magnitude. (b) Phase Angle.

simulations without using voltage measurements are tested for APF-FASE-II. The statistical MAE of the forecasted and estimated states under different configurations are shown in Figs. 4 and 5.

Through different configurations, the APF-FASE-II exhibits competitive forecasting and filtering results for phase angles containing more nonlinearities. Compared with the nonlinear-based EKF-FASE estimators, the neglected quadratic term in linear-based APF-FASE estimators inevitably dominates the minuscule voltage magnitude estimation error, i.e., difference at four decimal places. But it has no impact on handling nonlinear phase angles. As the number of forecasted power variations declines, the proposed prediction model based on the linear approximate power injection equation (*Remark 3*) is always demonstrated to maintain a better predictive capability than classical Holt's method, effectively relaxing the filtering pressure with measurement deficiencies. Even when APF-FASE-II excludes voltage measurements and relies solely on power flow measurements (*Remark 4*), the filtering results remain equivalent to APF-FASE-I. This promotes the proposed APF-FASE-II estimator as easy to implement for practical applications. Especially in real-world scenarios where real-time measurements are scarce, assembling a limited set of real-time power flow measurements and forecasted power injection variations can effectively track dynamic system states.

3) Sudden State Changes: To investigate the effectiveness of proposed method in handling sudden system state changes, the estimation process of bus 4 is still selected as an example to illustrate. Specifically, the real power injection at bus 4 is assumed to abruptly increase by ten times at the time sample $k = 32$. For EKF-FASE-I and APF-FASE-I, measurements of sudden changes in power injection are provided at the sudden moment; for EKF-FASE-II and APF-FASE-II, normal predicted power injection variations are still used in forecasting stage without sudden changing value provided. All other simulation settings remain unchanged from the normal operation. The comparison of the estimated voltage magnitude and phase angle is illustrated in Fig. 6.

It is obviously observed that all estimators have perceived and tracked the sudden state change. Due to the sudden change of real power at a load bus in the test system, the closely relevant dynamic estimation of voltage angle at bus 4 experienced a larger fluctuation than the voltage magnitude at the 32th time sample. Like the previous scenario results of limited real-time measurements, the APF-FASE-II obtains the most accurate phase angle and comparable voltage magnitude estimation results. The EKF-FASE-II, considering more nonlinear information in power flow measurements, has the most accuracy in estimating voltage magnitude. Even if the sudden power information is prior obtained at the changing moment, the voltage magnitude estimated by EKF-FASE-I and APF-FASE-I is still lower than that of APF-FASE-II. It further proves that the good tradeoff between the approximate power injection-based state forecasting and the approximate power flow-based filtering ability is enough to cope with sudden system state changes without excessive filtering correction.

4) Occurrence of Outliers: To demonstrate the robustness of the proposed method facing outliers occur in observations, we assume that all the measurements related to bus 17 are subject to cyber-attacks at the time sample $k = 40$. These include power injection measurements at P_{17}^{bad} and Q_{17}^{bad}, and power flow measurements at $P_{17,18}^{bad}$, $Q_{17,18}^{bad}$, $P_{17,33}^{bad}$, $Q_{17,33}^{bad}$, $P_{11,17}^{bad}$, and $Q_{11,17}^{bad}$, which are stealthily tampered with ten times from their original values. All other simulation settings remain unchanged from the normal operation. The comparison results are presented in Fig. 7, where the APF-FASE-II provides the most accurate estimation results of both voltage magnitude and phase angle at attacking time. Without considering the bad data detection scheme in power systems, the APF-FASE-II and EKF-FASE-II effectively weaken the adverse effect of abnormal measurement values on estimation results due to the accurate state prediction performance and the independent relationship on false power injection real-time measurements. In contrast, more vulnerabilities may be exposed by EKF-FASE-I and APF-FASE-I because of the necessary power injection measurements utilized in filtering stage.

Moreover, for APF-FASE-II, extensive simulations are per-

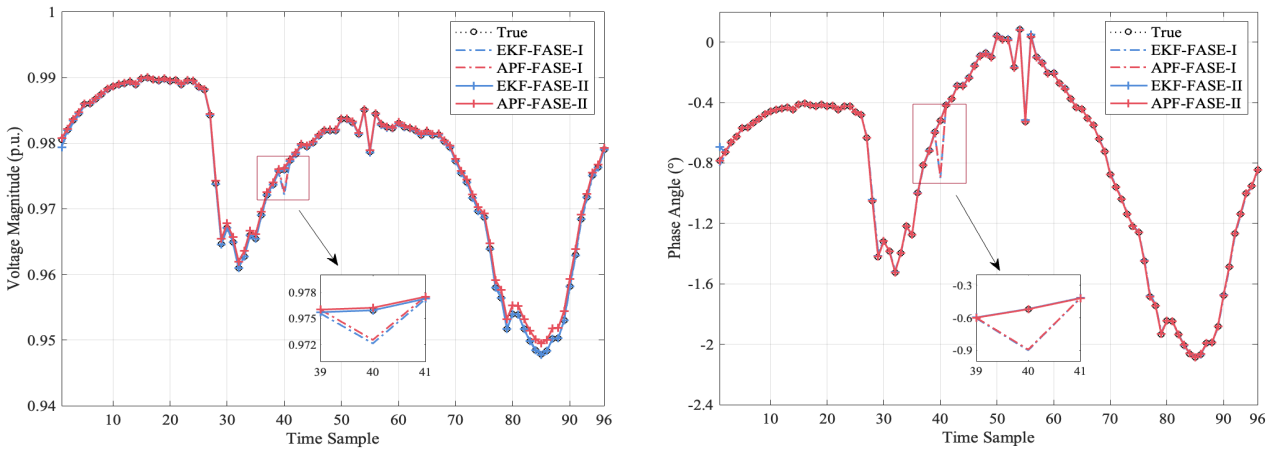

(a) Voltage Magnitude (b) Phase Angle

Fig. 7. Comparison results of estimating voltage magnitude and phase angle at bus 12 with outlier measurements. (a) Voltage Magnitude. (b) Phase Angle.

formed with false power injection pseudo-measurements in the prediction stage. With the increasing volume of false data, the statistical MAE and MRE results during the forecasting stage deteriorate accordingly. For example, as the proportion of false forecasted data rises from 25% to 75%, the MAE of forecasted states demonstrates an escalation from 0.0013 to 0.0044 for voltage magnitude and from 0.0429 to 0.1767 for phase angle, respectively. In any case, the accuracy of filtered states consistently aligns with the results observed under normal scenarios. The validity of the proposed measurement equation based on the approximate power flow model is demonstrated again.

VI. Conclusion and Future Work

Tackling the difficulties in determining the parameters of forecasting model and complicated selection of observations, an efficient approximate dynamic model for FASE is proposed in this research. The effectiveness of building a state transition model based on the approximate model from power injection measurements (*Remark 1 and 3*), and utilizing branch power flow as observations based on the approximate model from power flow measurements (*Remark 2 and 4*) are verified. The numerical results show that the proposed method can reduce the work required for model parameter adaptation and measurement collection while accurately and robustly obtaining system states, especially for voltage phase angles with more nonlinear factors. In this work, an equivalent single-phase model is adopted. Further attempts from this research will be developed on multi-phase and unbalanced distribution systems considering more complex conditions. Besides, it will be an interesting and valuable topic to explore the flexible distributed dynamic state estimation method for modern distribution systems based on the proposed lightweight structure combined with a decentralized perspective.

References

[1] A. Primadianto and C. -N. Lu, "A review on distribution system state estimation," *IEEE Trans. Power Syst.*, vol. 32, no. 5, pp. 3875-3883, Sept. 2017.

[2] Y. Wang, Y. Sun and V. Dinavahi, "Robust Forecasting-Aided State Estimation for Power System Against Uncertainties," *IEEE Trans. Power Syst.*, vol. 35, no. 1, pp. 691-702, Jan. 2020.

[3] S. Afzal, H. Mokhlis, H. A. Illias, N. Mansor and H. Shareef. "State-of-the-art review on power system resilience and assessment techniques," *IET Gener. Transm. Distrib.*, vol. 14, no. 25, pp. 6107-6121, Dec. 2020.

[4] J. Zhao, G. Zhang, Z. Y. Dong and M. La Scala, "Robust Forecasting Aided Power System State Estimation Considering State Correlations," *IEEE Trans. Smart Grid.*, vol. 9, no. 4, pp. 2658-2666, July 2018.

[5] M. Hassanzadeh, C. Y. Evrenosoğlu and L. Mili, "A Short-Term Nodal Voltage Phasor Forecasting Method Using Temporal and Spatial Correlation," *IEEE Trans. Power Syst.*, vol. 31, no. 5, pp. 3881-3890, Sept. 2016.

[6] J. Zhao et al., "Power System Dynamic State Estimation: Motivations, Definitions, Methodologies, and Future Work," *IEEE Trans. Power Syst.*, vol. 34, no. 4, pp. 3188-3198, July 2019.

[7] D. M. Falcão, P. A. Cooke, and A. Brameller, "Power system tracking state estimation and bad data processing," *IEEE Trans. Power App. Syst.*, vol. PAS-101, pp. 325–333, Feb. 1982.

[8] K. Nishiya, H. Takagi, J. Hasegawa, and T. Koike, "Dynamic state estimation for electric power systems—Introduction of a trend factor and detection of innovation processes," *Elect. Eng. Jpn.*, vol. 96, no. 5, pp. 79–87, May 1976.

[9] C. Chatfield, *The Analysis of Time Series: An Introduction*, ser. Texts in Statistical Science, 6th ed. London, U.K.: Chapman & Hall/CRC, 2003.

[10] M. B. Do Coutto Filho and J. C. Stacchini de Souza, "Forecasting-Aided State Estimation—Part I: Panorama," *IEEE Trans. Power Syst.*, vol. 24, no. 4, pp. 1667-1677, Nov. 2009.

[11] S. Sarri, L. Zanni, M. Popovic, J. -Y. Le Boudec and M. Paolone, "Performance Assessment of Linear State Estimators Using Synchrophasor Measurements," *Trans. Instrum. Meas.*, vol. 65, no. 3, pp. 535-548, Mar. 2016.

[12] X. Kong, X. Zhang, X. Zhang, C. Wang, H. -D. Chiang and P. Li, "Adaptive Dynamic State Estimation of Distribution Network Based on Interacting Multiple Model," *IEEE Trans. Sustain. Energy.*, vol. 13, no. 2, pp. 643-652, April 2022.

[13] L. Dang, B. Chen, S. Wang, W. Ma and P. Ren, "Robust Power System State Estimation With Minimum Error Entropy Unscented Kalman Filter," *Trans. Instrum. Meas.*, vol. 69, no. 11, pp. 8797-8808, Nov. 2020.

[14] Sharma, S. C. Srivastava and S. Chakrabarti, "A Cubature Kalman Filter Based Power System Dynamic State Estimator," *Trans. Instrum. Meas.*, vol. 66, no. 8, pp. 2036-2045, Aug. 2017.

[15] D. Hou, Y. Sun, L. Zhang and S. Wang, "Robust forecasting-aided state estimation considering uncertainty in distribution system," *CSEE J. Power Energy Syst.*.

[16] C. Cheng and X. Bai, "Robust Forecasting-Aided State Estimation in Power Distribution Systems With Event-Triggered Transmission and Reduced Mixed Measurements," *IEEE Trans. Power Syst.*,, vol. 36, no. 5, pp. 4343-4354, Sept. 2021.

[17] U. Eminoglu and M. H. Hocaoglu, "A new power flow method for radial

distribution systems including voltage dependent load models," *Elect. Power Syst. Res.*, vol. 76, pp. 106–114, 2005.

[18] S. Bolognani and S. Zampieri, "On the Existence and Linear Approximation of the Power Flow Solution in Power Distribution Networks," *IEEE Trans. Power Syst.*, vol. 31, no. 1, pp. 163-172, Jan. 2016.

[19] R. Deng, P. Zhuang and H. Liang, "False data injection attacks against state estimation in power distribution systems," *IEEE Trans. Smart Grid.*, vol. 10, no. 3, pp. 2871-2881, May. 2019.

[20] H. Ergun, J. Dave, D. Van Hertem and F. Geth, "Optimal Power Flow for AC–DC Grids: Formulation, Convex Relaxation, Linear Approximation, and Implementation," *IEEE Trans. Power Syst.*, vol. 34, no. 4, pp. 2980-2990, Jul. 2019.

[21] T Akbari and Bina M Tavakoli. "Linear approximated formulation of AC optimal power flow using binary discretisation," *IET Gener. Transm. Distrib.*, vol. 10, no. 5, pp. 1117-1123, 2016.

[22] Z Yang, H Zhong, Q Xia, A Bose and C Kang. "Optimal power flow based on successive linear approximation of power flow equations," *IET Gener. Transm. Distrib.*, vol. 10, no. 4, pp. 3654-3662, 2016.

[23] J. Li, M. Gao, B. Liu and Y. Cai, "Forecasting Aided Distribution Network State Estimation Using Mixed μPMU-RTU Measurements," *IEEE Syst. J.*, vol. 16, no. 4, pp. 6524-6534, Dec. 2022

[24] A. Sharma, S. C. Srivastava and S. Chakrabarti, "Testing and Validation of Power System Dynamic State Estimators Using Real Time Digital Simulator (RTDS)," *IEEE Trans. Power Syst.*, vol. 31, no. 3, pp. 2338-2347, May 2016.

[25] C. H. Ho, H. C. Wu, S. C. Chan and Y. Hou, "A Robust Statistical Approach to Distributed Power System State Estimation With Bad Data," *IEEE Trans. Smart Grid.*, vol. 11, no. 1, pp. 517-527, Jan. 2020.

[26] M. Beza and M. Bongiorno, "Application of Recursive Least Squares Algorithm With Variable Forgetting Factor for Frequency Component Estimation in a Generic Input Signal," *IEEE Trans. Ind. Appl.*, vol. 50, no. 2, pp. 1168-1176, March-April 2014.

[27] L. Hu, Z. Wang, I. Rahman and X. Liu, "A Constrained Optimization Approach to Dynamic State Estimation for Power Systems Including PMU and Missing Measurements," *IEEE Trans. Contr. Syst. Technol.*, vol. 24, no. 2, pp. 703-710, March 2016.

[28] Z. Cheng, H. Ren, B. Zhang and R. Lu, "Distributed Kalman Filter for Large-Scale Power Systems With State Inequality Constraints," *IEEE Trans. Ind. Electron.*, vol. 68, no. 7, pp. 6238-6247, July 2021.

[29] S. Dhople, S. Guggilam and Y. Chen, "Linear approximations to AC power flow in rectangular coordinates," in *53rd Annual Allerton Conference on Communication, Control, and Computing*, Urbana, IL, USA, 2015, pp. 211–217.

[30] R. Deng and H. Liang, "False data injection attacks with limited susceptance information and new countermeasures in smart grid," *IEEE Trans. Ind. Informat.*, vol. 15, no. 3, pp. 1619-1628, Mar. 2019.

[31] H. Li, Z. Ren, Y. Xu, W. Li and B. Hu, "A Multi-Data Driven Hybrid Learning Method for Weekly Photovoltaic Power Scenario Forecast," *IEEE Trans. Sustain. Energy.*, vol. 13, no. 1, pp. 91-100, Jan. 2022.

[32] J. Li, Z. Xu, J. Zhao and C. Zhang, "Distributed Online Voltage Control in Active Distribution Networks Considering PV Curtailment," *IEEE Trans. Ind. Informat.*, vol. 15, no. 10, pp. 5519-5530, Oct. 2019.

[33] M. Abdel-Nasser, K. Mahmoud and M. Lehtonen, "Reliable Solar Irradiance Forecasting Approach Based on Choquet Integral and Deep LSTMs," *IEEE Trans. Industr. Inform.*, vol. 17, no. 3, pp. 1873-1881, Mar. 2021.